Check for updates

Stability of Low-Reynolds-Number Separated Flow Around an Airfoil Near a Wavy Ground

Wei He* and Yu Guan†
Hong Kong University of Science and Technology, Clear Water Bay, Kowloon, Hong Kong, People's Republic of China
Vassilis Theofilis‡
University of Liverpool, Brownlow Hill, England L69 3GH, United Kingdom
and
Larry K. B. Li§
Hong Kong University of Science and Technology, Clear Water Bay, Kowloon, Hong Kong, People's Republic of China

DOI: 10.2514/1.J057544

In this numerical–theoretical study, a linear BiGlobal stability analysis of the steady massively separated flow around a NACA 4415 airfoil was performed at a low Reynolds number ($Re = 200$) and a high angle of attack ($\alpha = 18$ deg) close to a wavy ground, with a focus on the effect of three different types of stationary roughness: 1) a perfectly flat ground, 2) a wavy ground with small-amplitude undulations, and 3) a wavy ground with large-amplitude undulations. On increasing the undulation amplitude h_0 of the ground but keeping the mean ground clearance constant, it was found that the lift coefficient increased owing to an increase in the static pressure under the airfoil, which is reminiscent of the conventional ground effect over a flat surface. However, it was also found that the leading flow perturbation was the three-dimensional stationary global mode and not the two-dimensional traveling Kelvin–Helmholtz mode, contrary to the results of previous analogous studies of linear global instability of massively separated flow away from the ground. This study provides new insight into the stability of airfoil–ground flow systems at a low Reynolds number and a high angle of attack, contributing to a better understanding of the ground-effect aerodynamics of small insects and micro air vehicles flying over rough waters or complex terrain.

Downloaded by SOUTH UNIVERSITY OF SCIENCE AND on December 14, 2018 | http://arc.aiaa.org | DOI: 10.2514/1.J057544

Nomenclature

C_l	=	lift coefficient
C_p	=	static pressure coefficient
c	=	chord length of airfoil
H	=	clearance between mean ground profile and trailing edge of airfoil
h_0	=	peak-to-peak amplitude of ground undulations
L_z	=	spanwise wavelength
l	=	wavelength of ground undulations
$\boldsymbol{q}$	=	total field vector of velocity and pressure
$\bar{\boldsymbol{q}}$	=	base-flow vector
$\tilde{\boldsymbol{q}}$	=	small perturbation
$\hat{\boldsymbol{q}}$	=	amplitude function of perturbation
Re	=	Reynolds number based on airfoil chord
Sr	=	Strouhal number defined as $\omega_r/2\pi$
t	=	dimensionless time
U_∞	=	freestream velocity
x, y	=	streamwise and cross-stream directions in Cartesian coordinates
α	=	angle of attack
β	=	real spanwise wave number
ω	=	complex eigenvalue

Subscripts

i	=	imaginary part
r	=	real part

I. Introduction

WHEN an aircraft or a bird flies near the ground, it can experience an increase in aerodynamic efficiency [1], resulting in a higher lift-to-drag ratio [2] and a reduced mechanical power required for sustained flight [3]. This phenomenon is known as the ground effect [4] and has been studied in a variety of applications, ranging from flapping wing animals to unmanned aerial vehicles [5]. However, most of these studies have been carried out at moderate-to-high Reynolds numbers {$Re \sim \mathcal{O}(10^5$–$10^6)$ [6]}, at angles of attack α low enough to avoid stall, and with a ground surface that is perfectly flat. These conditions may not always coincide with reality. For example, when small insects or micro air vehicles fly over rough waters or complex terrain, the Reynolds number can drop to $\mathcal{O}(10^3$–$10^4)$ [7] or even $\mathcal{O}(10^2)$ [8], the angle of attack can be high enough to induce massive flow separation [9], and the ground may exhibit wavy undulations on its surface. Therefore, it is important to investigate the ground effect under these more realistic conditions.

Surprisingly, only a handful of studies have investigated airfoil flows over a wavy ground. Using Reynolds-averaged Navier–Stokes (NS) simulations, Yang et al. [10] examined the aerodynamic performance of a wing-in-ground-effect vehicle flying at $0.3c$ (c being the chord length) above a wavy ground at $Re = 6 \times 10^7$ and $\alpha = 5$ deg. The pressure under the wing was found to vary periodically in time, producing similarly periodic variations in the aerodynamic forces. However, compared with a flat ground, the wavy ground did not produce a marked difference in lift or drag, resulting in a relatively constant lift-to-drag ratio. By contrast, Wang [11] used the classical slender body theory to analyze the irrotational flow around a slender body moving over a wavy ground. The aerodynamic forces and moments were found to be highly dependent on the amplitude and wavelength of the ground undulations. The ground

Received 24 May 2018; revision received 8 October 2018; accepted for publication 8 October 2018; published online 10 December 2018. Copyright © 2018 by the American Institute of Aeronautics and Astronautics, Inc. All rights reserved. All requests for copying and permission to reprint should be submitted to CCC at www.copyright.com; employ the ISSN 0001-1452 (print) or 1533-385X (online) to initiate your request. See also AIAA Rights and Permissions www.aiaa.org/randp.

*Research Associate, Department of Mechanical and Aerospace Engineering; mewhe@ust.hk.
†Ph.D. Candidate, Department of Mechanical and Aerospace Engineering.
‡Chair Professor, School of Engineering. Associate Fellow AIAA.
§Assistant Professor, Department of Mechanical and Aerospace Engineering.

Downloaded by SOUTH UNIVERSITY OF SCIENCE AND on December 14, 2018 | http://arc.aiaa.org | DOI: 10.2514/1.J057544

effect was found to be particularly strong when the undulation amplitude became comparable to the ground clearance and/or when the undulation wavelength became comparable to the body length (chord). However, to date, the effect of a wavy ground on the massively separated flow around an airfoil at a low Reynolds number and a high angle of attack has yet to be explored, particularly for undulation wavelengths shorter than the chord length. This is the focus of the present study.

Another unique aspect of the present study concerns the introduction of three-dimensionality to this problem, through the use of global flow stability analysis. To develop effective control strategies to suppress flow separation and improve aerodynamic performance requires a sound understanding of the instability characteristics of the base flow [12–18]. Linear stability analysis has been used to successfully predict the primary stability of two- and three-dimensional flows [19]. For example, by combining local and global linear stability analyses on the flow around airfoils at a low angle of attack, Theofilis et al. [20] and Lin and Pauley [21] were able to attribute the dominant perturbation to the Kelvin–Helmholtz (KH) mode. Likewise, at a high angle of attack, a similar dominance by the KH mode was found in the massively separated flow around a series of NACA airfoils at a low Reynolds number [22,23]. For steady separated flow around an airfoil at a low Reynolds number, Kitsios et al. [24] observed the existence of three-dimensional stationary modes, which were first reported by Theofilis et al. [25] in a flat-plate boundary layer. However, these three-dimensional stationary modes have recently been found to be less unstable than the two-dimensional KH mode [23]. A similar conclusion was reached by He et al. [26], who analyzed both the primary and secondary instabilities of the unsteady separated flow around a NACA 4415 airfoil at $300 \leq Re \leq 1000$ and $\alpha = 20$ deg. The airfoil was positioned at a nondimensional height (based on the chord length) of $0.2 \leq H \leq \infty$ above two different types of flat ground: a stationary ground and a moving ground. Results from the latter linear stability analysis showed that, consistent with previous studies and regardless of ground type, the two-dimensional KH mode always dominates over the three-dimensional stationary global mode. However, no attempt was made to analyze the stability of the flow at Reynolds-number values below that required for the onset of unsteady vortex shedding or in the presence of a wavy ground.

In this numerical–theoretical study, we perform a linear BiGlobal stability analysis of the steady but massively separated flow around a NACA 4415 airfoil at a low Reynolds number ($Re = 200$) and a high angle of attack ($\alpha = 18$ deg), with a focus on the effect of three different types of stationary ground: 1) a perfectly flat ground, 2) a wavy ground with small-amplitude undulations, and 3) a wavy ground with large-amplitude undulations. The aim was to see whether and how the presence of short-wavelength undulations of different amplitudes on the ground can influence the structure and stability of the flow, particularly at a Reynolds-number value below that required for the onset of unsteady vortex shedding.

II. Problem Formulation

A. Wavy Ground Definition

The wavy ground is defined by a set of cosine functions:

$$h(x) \equiv \frac{h_0}{2}\left(1 + \cos\frac{2\pi x}{l}\right), \qquad x \in [0, l] \tag{1}$$

in which l is the wavelength, and $h_0/2$ is the amplitude of the ground undulations. The wave trough is fixed at $h = 0$, but the wave crest is set by $h = h_0$. When $h_0 = 0$, the ground defaults to a flat surface, as shown in Fig. 1. With this ground definition [Eq. (1)], if an airfoil were positioned at a fixed height above the datum $h = 0$, increasing h_0 would have the side effect of reducing the mean ground clearance H, which is defined as the vertical distance between the trailing edge of the airfoil and the mean ground profile (horizontal dashed lines in Fig. 1). Therefore, to enable an investigation of the sole effect of h_0, we shift the airfoil up as h_0 increases, such that H is kept constant at 0.2. All length scales are nondimensionalized by the chord length c.

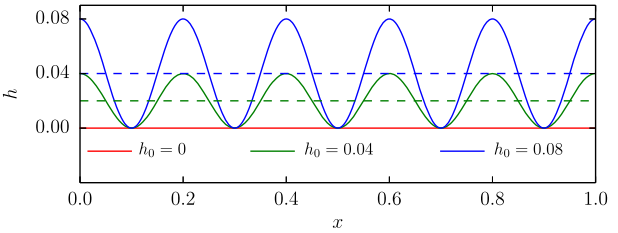

Fig. 1 Three ground profiles considered in this study.

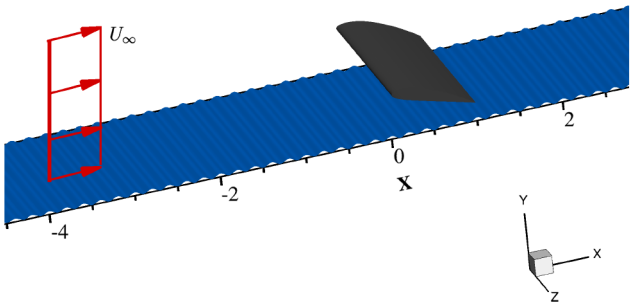

Fig. 2 Perspective view of the airfoil–ground system.

A perspective view of this airfoil–ground system is shown in Fig. 2, in which the airfoil (NACA 4415) and wavy ground are colored in black and blue, respectively.

B. Linear Stability Theory

A linear BiGlobal stability analysis was performed to investigate the evolution of three-dimensional perturbations on a nominally two-dimensional base flow. The flow is governed by the nondimensional incompressible NS and continuity equations:

$$\partial_t \boldsymbol{u} + \boldsymbol{u}\cdot\nabla\boldsymbol{u} = -\nabla p + Re^{-1}\nabla^2\boldsymbol{u}, \qquad \nabla\cdot\boldsymbol{u} = 0 \tag{2}$$

in which the Reynolds number is defined as $Re \equiv U_\infty c/\nu$, with U_∞ as the freestream velocity, c the chord length, and ν the kinematic viscosity. The dimensionless velocity and pressure are $\boldsymbol{q}(x, y, z, t) = (\boldsymbol{u}, p)^T = (u, v, w, p)^T$, which consists of a base-flow component $\bar{\boldsymbol{q}}$ and a small perturbation $\tilde{\boldsymbol{q}}$. In incompressible flow, the pressure perturbation can be expressed as $\tilde{p} = \nabla^{-2}(\nabla\cdot(\tilde{\boldsymbol{u}}\cdot\nabla\tilde{\boldsymbol{u}} + \tilde{\boldsymbol{u}}\cdot\nabla\bar{\boldsymbol{u}}))$, leading to the linearized NS equation:

$$\partial_t\tilde{\boldsymbol{u}} = \mathcal{L}\tilde{\boldsymbol{u}} \tag{3}$$

in which $\mathcal{L}$ is a linear operator. In a BiGlobal stability analysis, the small three-dimensional perturbations are spanwise homogeneous, $\tilde{\boldsymbol{u}}(x, y, z, t) = \hat{\boldsymbol{u}}(x, y)e^{i(\beta z-\omega t)} + \text{c.c.}$, in which $\hat{\boldsymbol{u}}$ is the amplitude function, $\beta \equiv 2\pi/L_z$ is the wave number along the spanwise periodic length L_z, and c.c. is a complex conjugate to ensure real-valued perturbations. Here, ω is the complex eigenvalue of the matrix $\mathcal{A}$ in $\mathcal{A}\tilde{\boldsymbol{u}} = -i\omega\tilde{\boldsymbol{u}}$, which is derived from Eq. (3).

Table 1 Numerical schemes used for the base-flow and stability analyses

	Projection method	Time integration	Eigenvalue algorithm
Base flow	CG	IMEX2	— —
Direct analysis	CG	IMEX2	Arnoldi
Adjoint analysis	CG	IMEX2	Arnoldi

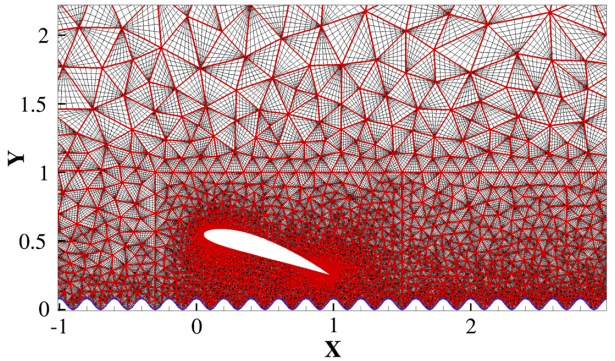

Fig. 3 Zoomed-in view of the computational domain around the airfoil.

Downloaded by SOUTH UNIVERSITY OF SCIENCE AND on December 14, 2018 | http://arc.aiaa.org | DOI: 10.2514/1.J057544

C. Numerical Setup

To compute the base flow, we used direct numerical simulations (DNSs) of the NS equations in two dimensions. We did this at $Re = 200$ and $\alpha = 18$ deg because, as will be shown next, this Reynolds-number value is low enough to avoid unsteady vortex shedding, and this angle-of-attack value is high enough to induce massive flow separation. We set the wavelength of the ground undulations to be $l = 0.2$ (one-fifth of the chord length), but explored three different undulation amplitudes (see Fig. 1): $h_0 = 0$, 0.04, and 0.08. The computational domain, defined by $\{x, y\} = \{[-5:8.5] \times [0:5]\}$, was discretized into $\mathcal{O}(5400)$ triangular macroelements using Gmsh [27]. Along the ground, each period of the wavy undulating surface was defined by six second-order curves. This macromesh was then imported to Nektar++ [28], an open-source spectral/hp element solver [29]. In this study, we used the continuous Galerkin (CG) method and a second-order implicit–explicit (IMEX2) time-integration scheme to solve the incompressible NS equations. The numerical schemes used for the base-flow and stability analyses are summarized in Table 1. Figure 3 shows a zoomed-in view of the mesh around the airfoil–ground system after refinement by a spectral polynomial of order $p = 7$. (Each element is outlined by red lines.) The inflow length ($5c$) is similar to that of previous studies [30], and is long enough for the base-flow and stability analyses to converge, as will be demonstrated next in a sensitivity analysis.

For numerical stability, a robust outflow boundary condition is applied to the top and right edges of the computational domain [31]. A uniform inflow condition ($U_\infty = 1$; $\partial_n p = 0$) is applied to the left edge. A no-slip wall condition ($\boldsymbol{u} = 0$) is applied to the airfoil surface. For the perturbations, the inflow and wall conditions are of the homogeneous Dirichlet type ($\hat{\boldsymbol{u}} = 0$), and the outflow condition is of the homogeneous Neumann type ($\partial_n \hat{\boldsymbol{u}} = 0$). The wavy ground is modeled as a stationary stress-free wall. In most flight conditions, an insect or micro air vehicle would fly over a stationary ground, resulting in a time-dependent phase relationship between the airfoil and the undulations on the ground. In our study, however, we intentionally kept this phase relationship constant so as to simplify the problem. Although this approach is only partially representative of flight over a wavy ground, it nevertheless enables the steady effect of a wavy ground to be explored, setting the scene for future studies involving a time-dependent phase relationship.

III. Results and Discussion

A. Base Flow

Table 2 shows the results of a grid independence study for $H = 0.18$, which requires a higher-resolution mesh than for $H = 0.2$. Convergence is assessed by increasing the polynomial order of the mesh (p) and monitoring five indicators: 1) the lift coefficient C_l; 2) the drag coefficient C_d; and 3–5) the spanwise vorticity $\omega_z = \partial v/\partial x - \partial u/\partial y$ at three different locations around the airfoil, which are near the leading edge $[P_1(0.1, 0.6)]$, near the trailing edge $[P_2(1.0, 0.22)]$, and in the separation bubble $[P_3(1.1, 0.55)]$. The relative error in each of these indicators (ϵ_{C_l}, ϵ_{C_d}, and ϵ_{ω_z}) is shown in Table 2. Of all the indicators examined, ω_z is the most sensitive to changes in grid resolution. Nevertheless, the maximum relative error in ω_z is still relatively small, at less than 1.1% for $p = 7$. Therefore, to balance the numerical accuracy and the computational cost, we used $p = 7$ in our base-flow simulations and stability analysis.

Figure 4 shows DNS streamlines and spanwise vorticity contours ($-5 \leq \omega_z \leq 5$) around the airfoil at $Re = 200$ and $\alpha = 18$ deg for three different types of ground, from left to right: 1) a flat ground, $h_0 = 0$; 2) a wavy ground with small-amplitude undulations, $h_0 = 0.04$; and 3) a wavy ground with large-amplitude undulations, $h_0 = 0.08$. For all three cases, the flow is steady in time, confirming that Reynolds number is indeed low enough to avoid unsteady vortex shedding. There is massive flow separation behind the airfoil, resulting in a robust separation bubble with two large recirculation zones. As the undulation amplitude h_0 of the ground increases, the length of the separation bubble also increases, but its overall structure remains largely unchanged. Figure 5 shows the static pressure coefficient C_p on the airfoil surface. As h_0 increases, C_p remains relatively constant on the suction side of the airfoil, but increases slightly on the pressure side, especially near the midchord location, resulting in an increase in the lift coefficient C_l, as shown in the legend of Fig. 5.

B. Stability Analysis

Direct stability analysis is performed by finding the least stable eigenvalues of $\mathcal{A}$ using the Arnoldi iteration in a time-forward mapping scheme, implemented in Nektar++. Adjoint stability analysis is performed by solving the adjoint operator of Eq. (3) in a time-backward mapping scheme. Both types of stability analysis give the same eigenvalues if the problem is domain independent. We used this feature to demonstrate that our computational domain is sufficiently large. Table 3 shows a sensitivity analysis performed on the size of the computational domain for a sample flow condition ($h_0 = 0.04$; $\beta = 0$). The agreement in growth rate and frequency between the direct and adjoint modes is good, confirming that the computational domain is large enough for the instability properties to converge.

Figure 6 shows the growth rate (ω_i) and Strouhal number ($Sr \equiv \omega_r/2\pi$) as a function of the spanwise wave number β for the flow conditions of Fig. 4. Two different classes of instability modes can be identified: 1) two-dimensional traveling KH modes (denoted by hollow markers), for which $Sr > 0$; and 2) three-dimensional stationary global modes (denoted by filled markers), for which $Sr = 0$ (not plotted). As mentioned earlier, similar modes have been identified before in both steady [24] and unsteady [20] separated flows around an airfoil with [26] and without [23,32] the ground effect. However, in contrast to those earlier studies, in which the KH

Table 2 Grid independence study based on the relative errors in C_l, C_d, and ω_z at three different locations around the airfoil

p	ω_z at P_1	ω_z at P_2	ω_z at P_3	ϵ_{ω_z}, %	C_d	ϵ_{C_d}, %	C_l	ϵ_{C_l}, %
5	−17.674540	−2.281345	−2.174560	3.15	0.5166	0.04	1.4172	0.04
7	−17.673402	−2.380518	−2.173184	1.06	0.5168	0.02	1.4166	0.02
9	−17.670292	−2.355664	−2.174399	— —	0.5170	— —	1.4168	— —

The relative error in ω_z is the maximum value found across the three sampling locations.

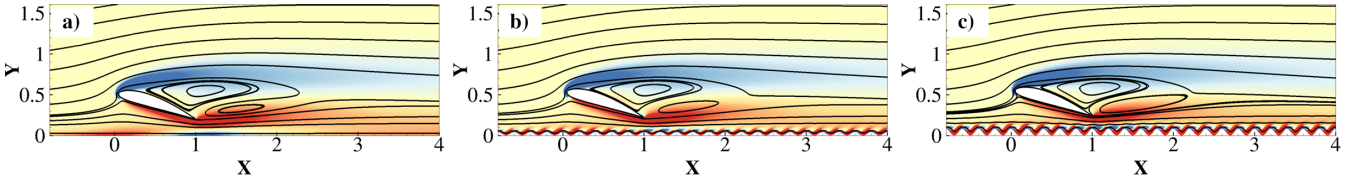

Fig. 4 DNS streamlines and spanwise vorticity distribution around the airfoil-ground system.

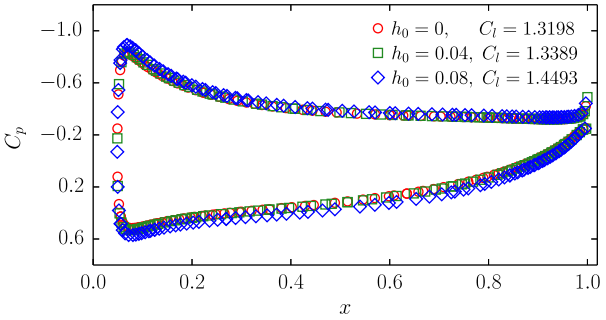

Fig. 5 Static pressure coefficient on the airfoil surface at the conditions of Fig. 4.

Table 3 Sensitivity analysis based on the size of the computational domain for a sample flow condition ($h_0 = 0.04; \beta = 0$)

Mode	ω_i	ω_r
Direct	−0.10434	2.2171
Adjoint	−0.10293	2.2220

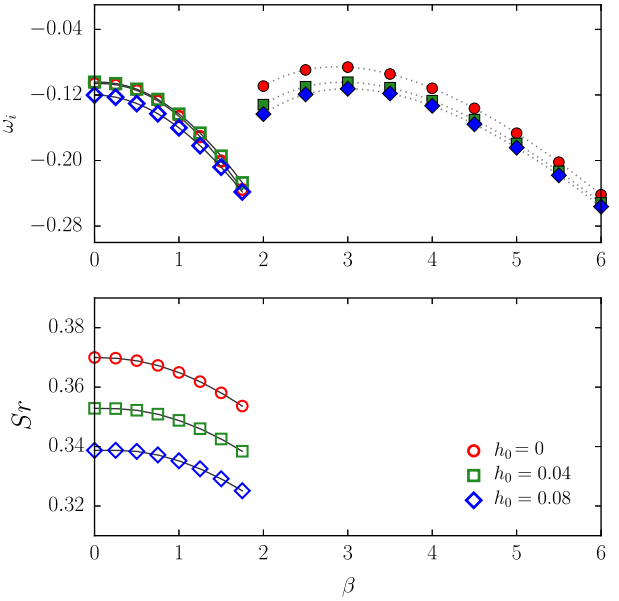

Fig. 6 Linear BiGlobal stability analysis at the flow conditions of Fig. 4.

mode was always found to dominate over the stationary mode, here, we found the opposite behavior: the KH mode is more stable than the stationary mode. The former is dominant at small wave numbers ($\beta \approx 0$), whereas the latter is dominant at large wave numbers ($\beta \approx 3$). As h_0 increases, the frequency of the KH mode decreases. The growth rates of both the KH and stationary modes also decrease, but to a lesser extent, with the former mode being slightly more stable than the latter mode. All the growth rates of the perturbations are negative, implying that both the KH and stationary modes decay in the long-time asymptotic limit.

Figure 7 shows the three components of the perturbation amplitude function $\hat{\boldsymbol{q}}$ at $\beta = 1$ (KH mode) and $\beta = 3$ (stationary mode) for $h_0 = 0.04$; these components are normalized by their respective maximum velocities. As mentioned earlier, the KH mode is stable at this Reynolds number ($Re = 200$). However, a recent work by He et al. [26] on the separated flow around a NACA 4415 airfoil above a flat ground has shown that, when the Reynolds number exceeds roughly 500, the KH mode becomes unstable, destroying the steady separation bubble behind the airfoil and producing large-scale vortex shedding downstream at a well-defined frequency. Thus, at higher values of Reynolds number, the KH mode is expected to cause the airfoil wake to transition from a spatial amplifier of extrinsic perturbations to a self-excited oscillator with an intrinsic natural frequency [33]. Such a transition, which is often referred to as a Hopf bifurcation [34], has been reported before not only in airfoil wakes [35], but also in cylinder wakes [36], crossflowing jets [37], and low-density jets [38–40]. To examine the evolution of the optimal perturbations, we performed a transient growth analysis by estimating the energy gain $G(\tau)$ over a time horizon τ. Figure 8 shows that $G(\tau)$ grows to $\mathcal{O}(10)$ over a short time horizon, and then decays linearly, indicating the presence of convective instability [23].

Unlike the spatially growing stationary mode identified by He et al. [23], here, the spatial structures of the stationary mode dominate the wake behind the airfoil, and then decay downstream. The streamwise perturbation is consistently stronger than the other two components. The perturbation functions for the other two values of h_0 (0 and 0.08) are qualitatively similar to that for $h_0 = 0.04$ (Fig. 7). Figure 9 shows a three-dimensional reconstruction of the least stable stationary mode at $\beta = 3$, as represented by the λ_2 criterion and the streamwise vorticity (transparent isocontours). It can be seen that the vortical structure of the perturbation is most complex behind the trailing edge of the airfoil, with two long stable vortices developing downstream. The streamwise velocity of the stationary mode is visualized by dashed and solid lines ($-0.01 \le \hat{u} \le 0.01$) in a vertical plane at $x = 4$.

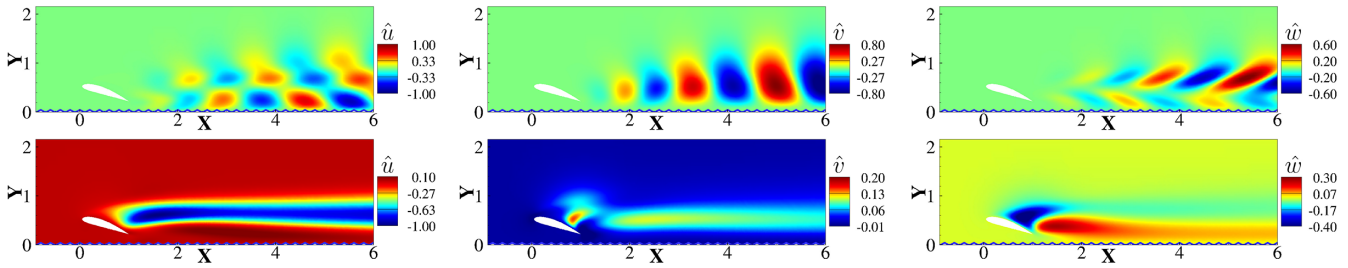

Fig. 7 Normalized perturbation amplitude function $\hat{q}$ at $h_0 = 0.04$ for (top row) the KH mode and (bottom row) the stationary mode.

Downloaded by SOUTH UNIVERSITY OF SCIENCE AND on December 14, 2018 | http://arc.aiaa.org | DOI: 10.2514/1.J057544

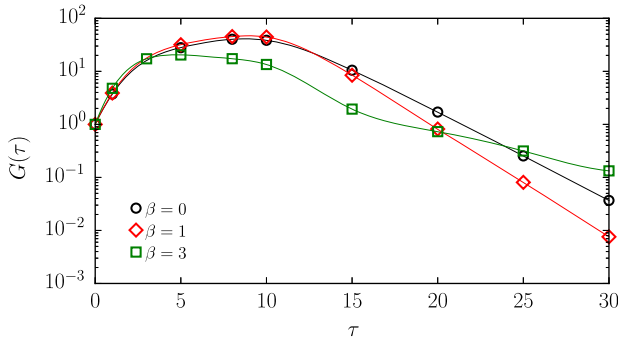

Fig. 8 Transient growth of the optimal perturbations with respect to the time horizon.

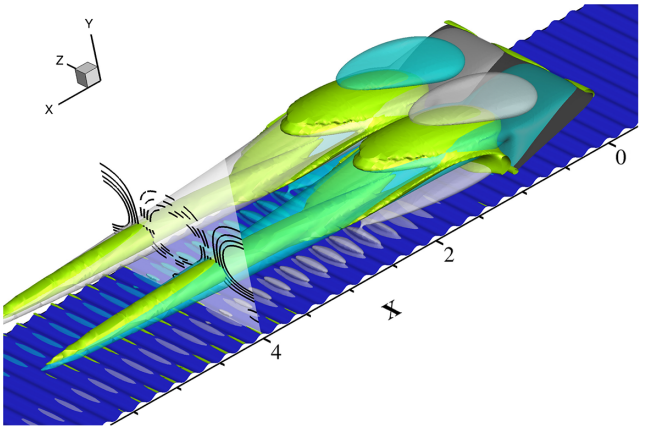

Fig. 9 Three-dimensional reconstruction of the least stable stationary mode ($\beta = 3$).

IV Conclusions

A linear BiGlobal stability analysis of the steady massively separated flow around a NACA 4415 airfoil has been performed at a low Reynolds number ($Re = 200$) and a high angle of attack ($\alpha = 18$ deg), with a focus on the effect of three different types of stationary ground: 1) a perfectly flat ground, 2) a wavy ground with small-amplitude undulations, and 3) a wavy ground with large-amplitude undulations. For a fixed ground clearance ($H = 0.2$), it was found that increasing the undulation amplitude h_0 of the ground leads to a higher lift coefficient, similar to the classical ground effect over a flat surface. However, it was also found that the leading flow perturbation is the three-dimensional stationary global mode and not the two-dimensional traveling KH mode, contrary to previous analogous studies away from the ground. Increasing h_0 was found to reduce the growth rates and frequencies of the KH and stationary modes. This work shows that the spanwise periodicity length of the leading stationary disturbances in the wake of an airfoil is of $\mathcal{O}(2c)$. This study provides new insight into the stability of airfoil–ground flow systems at a low Reynolds number and a high angle of attack, contributing to an improved understanding of natural flyers and micro air vehicles. Possible directions for future work include adopting a dynamic mesh so that the effect of a time-dependent phase relationship between the airfoil and the wavy ground can be explored.

Acknowledgments

This work was supported by the Research Grants Council of Hong Kong (project numbers 16235716 and 26202815) and by the computational resources (Barkla) of the University of Liverpool.

References

[1] Rozhdestvensky, K. V., "Wing-in-Ground Effect Vehicles," *Progress in Aerospace Sciences*, Vol. 42, No. 3, 2006, pp. 211–283. doi:10.1016/j.paerosci.2006.10.001

[2] Hainsworth, F. R., "Induced Drag Savings from Ground Effect and Formation Flight in Brown Pelicans," *Journal of Experimental Biological Sciences*, Vol. 135, No. 1, 1988, pp. 431–444.

[3] Rayner, J. M., "On the Aerodynamics of Animal Flight in Ground Effect," *Philosophical Transactions of the Royal Society B: Biological Sciences*, Vol. 334, No. 1269, 1991, pp. 119–128. doi:10.1098/rstb.1991.0101

[4] Halloran, M., and O'Meara, S., "Wing in Ground Effect Craft Review," Defence Science and Technology Organisation Canberra (Australia), DSTO-GD-0201, Canberra, Australia, 1999.

[5] Qu, Q., and Agarwal, R. K., *Chord-Dominated Ground-Effect Aerodynamics of Fixed-Wing UAVs*, John Wiley & Sons, West Sussex, U.K., 2017, pp. 201–254. doi:10.1002/9781118928691.ch6

[6] Ahmed, M. R., Takasaki, T., and Kohama, Y., "Aerodynamics of a NACA 4412 Airfoil in Ground Effect," *AIAA Journal*, Vol. 45, No. 1, 2007, pp. 37–47. doi:10.2514/1.23872

[7] Heathcote, S., and Gursul, I., "Flexible Flapping Airfoil Propulsion at Low Reynolds Numbers," *AIAA Journal*, Vol. 45, No. 5, 2007, pp. 1066–1079. doi:10.2514/1.25431

[8] Birch, J. M., and Dickinson, M. H., "Spanwise Flow and the Attachment of the Leading-Edge Vortex on Insect Wings," *Nature*, Vol. 412, No. 6848, 2001, pp. 729–733. doi:10.1038/35089071

[9] Shyy, W., Lian, Y., Tang, J., Liu, H., Trizila, P., Stanford, B., Bernal, L., Cesnik, C., Friedmann, P., and Ifju, P., "Computational Aerodynamics of Low Reynolds Number Plunging, Pitching and Flexible Wings for MAV Applications," *46th AIAA Aerospace Sciences Meeting and Exhibit*, AIAA Paper 2008-523, Jan. 2008. doi:10.2514/6.2008-523

[10] Yang, W., Ying, C., and Yang, Z., "Aerodynamics Study of WIG Craft Near Curved Ground," *Journal of Hydrodynamics, Ser. B*, Vol. 22, No. 5, 2010, pp. 371–376. doi:10.1016/S1001-6058(09)60221-3

[11] Wang, Q. X., "Analyses of a Slender Body Moving Near a Curved Ground," *Physics of Fluids A*, Vol. 17, No. 9, 2005, Paper 097102. doi:10.1063/1.2034867

[12] Blackburn, H. M., Sherwin, S. J., and Barkley, D., "Convective Instability and Transient Growth in Steady and Pulsatile Stenotic Flows," *Journal of Fluid Mechanics*, Vol. 607, Jan. 2008, pp. 267–277. doi:10.1017/S0022112008001717

[13] Hill, D., "A Theoretical Approach for Analyzing the Restabilization of Wakes," *30th Aerospace Sciences Meeting and Exhibit*, AIAA Paper 1992-0067, 1992. doi:10.2514/6.1992-67

[14] Bisek, N. J., Rizzetta, D. P., and Poggie, J., "Plasma Control of a Turbulent Shock Boundary-Layer Interaction," *AIAA Journal*, Vol. 51, No. 8, 2013, pp. 1789–1804. doi:10.2514/1.J052248

[15] Luchini, P., and Bottaro, A., "Adjoint Equations in Stability Analysis," *Annual Review of Fluid Mechanics*, Vol. 46, Jan. 2014, pp. 493–517. doi:10.1146/annurev-fluid-010313-141253

[16] Sipp, D., and Schmid, P., "Linear Closed-Loop Control of Fluid Instabilities and Noise-Induced Perturbations: A Review of Approaches and Tools," *Applied Mechanics Reviews*, Vol. 68, No. 2, 2016, Paper 020801. doi:10.1115/1.4033345

[17] He, W., Tendero, J. Á., Paredes, P., and Theofilis, V., "Linear Instability in the Wake of an Elliptic Wing," *Theoretical and Computational Fluid Dynamics*, Vol. 31, Nos. 5–6, 2017, pp. 483–504. doi:10.1007/s00162-016-0400-2

[18] Ma, B., and Yin, S., "Vortex Oscillations Around a Hemisphere-Cylinder Body with a High Fineness Ratio," *AIAA Journal*, Vol. 56, No. 4, 2018, pp. 1402–1420. doi:10.2514/1.J056047

[19] Taira, K., Brunton, S. L., Dawson, S. T. M., Rowley, C. W., Colonius, T., McKeon, B. J., Schmidt, O. T., Gordeyev, S., Theofilis, V., and Ukeiley, L. S., "Modal Analysis of Fluid Flows: An Overview," *AIAA Journal*, Vol. 55, No. 12, 2017, pp. 4013–4041. doi:10.2514/1.J056060

[20] Theofilis, V., Barkley, D., and Sherwin, S., "Spectral/hp Element Technology for Global Flow Instability and Control," *Aeronautical Journal*, Vol. 106, No. 1065, 2002, pp. 619–625. doi:10.1017/S0001924000018285

[21] Lin, J. C. M., and Pauley, L. L., "Low-Reynolds-Number Separation on an Airfoil," *AIAA Journal*, Vol. 34, No. 8, 1996, pp. 1570–1577. doi:10.2514/3.13273

Downloaded by SOUTH UNIVERSITY OF SCIENCE AND on December 14, 2018 | http://arc.aiaa.org | DOI: 10.2514/1.J057544

[22] Brehm, C., and Fasel, H. F., "BiGlobal Stability Analysis as an Initial Value Problem for a Stalled Airfoil," *41st AIAA Fluid Dynamics Conference and Exhibit*, AIAA Paper 2011-3569, June 2011. doi:10.2514/6.2011-3569

[23] He, W., Gioria, R. S., Pérez, J. M., and Theofilis, V., "Linear Instability of Low Reynolds Number Massively Separated Flow Around Three NACA Airfoils," *Journal of Fluid Mechanics*, Vol. 811, Jan. 2017, pp. 701–741. doi:10.1017/jfm.2016.778

[24] Kitsios, V., Rodríguez, D., Theofilis, V., Ooi, A., and Soria, J., "BiGlobal Stability Analysis in Curvilinear Coordinates of Massively Separated Lifting Bodies," *Journal of Computational Physics*, Vol. 228, No. 19, 2009, pp. 7181–7196. doi:10.1016/j.jcp.2009.06.011

[25] Theofilis, V., Hein, S., and Dallmann, U., "On the Origins of Unsteadiness and Three-Dimensionality in a Laminar Separation Bubble," *Philosophical Transactions of the Royal Society A: Mathematical, Physical and Engineering Sciences*, Vol. 358, No. 1777, 2000, pp. 3229–3246. doi:10.1098/rsta.2000.0706

[26] He, W., Yu, P., and Li, L. K. B., "Ground Effects on the Stability of Separated Flow Around a NACA 4415 Airfoil at Low Reynolds Numbers," *Aerospace Science and Technology*, Vol. 72, Jan. 2018, pp. 63–76. doi:10.1016/j.ast.2017.10.039

[27] Geuzaine, C., and Remacle, J. F., "Gmsh: A Three-Dimensional Finite Element Mesh Generator with Built-in Pre- and Post-Processing Facilities," *International Journal for Numerical Methods in Engineering*, Vol. 79, No. 11, 2009, pp. 1309–1331. doi:10.1002/nme.v79:11

[28] Cantwell, C., Moxey, D., Comerford, A., Bolis, A., Rocco, G., Mengaldo, G., Grazia, D. D., Yakovlev, S., Lombard, J., and Ekelschot, D., et al., "Nektar++: An Open-Source Spectral/hp Element Framework," *Computer Physics Communications*, Vol. 192, July 2015, pp. 205–219. doi:10.1016/j.cpc.2015.02.008

[29] Patera, A. T., "A Spectral Element Method for Fluid Dynamics: Laminar Flow in a Channel Expansion," *Journal of Computational Physics*, Vol. 54, No. 3, 1984, pp. 468–488. doi:10.1016/0021-9991(84)90128-1

[30] Tombouldides, A. G., and Orszag, S. A., "Numerical Investigation of Transitional and Weak Turbulent Flow Past a Sphere," *Journal of Fluid Mechanics*, Vol. 416, Aug. 2000, pp. 45–73. doi:10.1017/S0022112000008880

[31] Dong, S., Karniadakis, G., and Chryssostomidis, C., "A Robust and Accurate Outflow Boundary Condition for Incompressible Flow Simulations on Severely-Truncated Unbounded Domains," *Journal of Computational Physics*, Vol. 261, March 2014, pp. 83–105. doi:10.1016/j.jcp.2013.12.042

[32] Zhang, W., and Samtaney, R., "BiGlobal Linear Stability Analysis on Low-Re Flow Past an Airfoil at High Angle of Attack," *Physics of Fluids*, Vol. 28, April 2016, Paper 044105. doi:10.1063/1.4945005

[33] Huerre, P., and Monkewitz, P. A., "Local and Global Instabilities in Spatially Developing Flows," *Annual Review of Fluid Mechanics*, Vol. 22, Jan. 1990, pp. 473–537. doi:10.1146/annurev.fl.22.010190.002353

[34] Hilborn, R., *Chaos and Nonlinear Dynamics*, 2nd ed., Oxford Univ. Press, Oxford, England, U.K., 2000, Chap. 3.

[35] Deane, A. E., and Mavriplis, C., "Low-Dimensional Description of the Dynamics in Separated Flow Past Thick Airfoils," *AIAA Journal*, Vol. 32, No. 6, 1994, pp. 1222–1227. doi:10.2514/3.12123

[36] Provansal, M., Mathis, C., and Boyer, L., "Bénard-Von Kármán Instability: Transient and Forced Regimes," *Journal of Fluid Mechanics*, Vol. 182, Sept. 1987, pp. 1–22. doi:10.1017/S0022112087002222

[37] Davitian, J., Getsinger, D., Hendrickson, C., and Karagozian, A. R., "Transition to Global Instability in Transverse-Jet Shear Layers," *Journal of Fluid Mechanics*, Vol. 661, Oct. 2010, pp. 294–315. doi:10.1017/S0022112010003046

[38] Li, L. K. B., and Juniper, M. P., "Lock-in and Quasiperiodicity in a Forced Hydrodynamically Self-Excited Jet," *Journal of Fluid Mechanics*, Vol. 726, July 2013, pp. 624–655. doi:10.1017/jfm.2013.223

[39] Li, L. K. B., and Juniper, M. P., "Phase Trapping and Slipping in a Forced Hydrodynamically Self-Excited Jet," *Journal of Fluid Mechanics*, Vol. 735, No. R5, Nov. 2013, pp. 1–11. doi:10.1017/jfm.2013.533

[40] Zhu, Y., Gupta, V., and Li, L. K. B., "Onset of Global Instability in Low-Density Jets," *Journal of Fluid Mechanics*, Vol. 828, No. R1, Oct. 2017, pp. 1–12. doi:10.1017/jfm.2017.555

P. Givi
Associate Editor

Downloaded by SOUTH UNIVERSITY OF SCIENCE AND on December 14, 2018 | http://arc.aiaa.org | DOI: 10.2514/1.J057544